In-vivo Performance of Photovoltaic Subretinal Prosthesis

Yossi Mandel[1,2], Georges Goetz[1,3], Daniel Lavinsky[2], Phil Huie[1,2], Keith Mathieson[4], Lele Wang[3], Theodore Kamins[3], Richard Manivanh[2], James Harris[3], Daniel Palanker[1,2]
[1]Hansen Experimental Physics Laboratory, Stanford University, Stanford, CA, 94305, USA
[2]Department of Ophthalmology, Stanford University, Stanford, CA, 94305, USA
[3]Department of Electrical Engineering, Stanford University, Stanford, CA, 94305, USA
[4]Institute of Photonics, University of Strathclyde, Glasgow, Scotland, G4 0NW

ABSTRACT

We have developed a photovoltaic retinal prosthesis, in which camera-captured images are projected onto the retina using pulsed near-IR light. Each pixel in the subretinal implant directly converts pulsed light into local electric current to stimulate the nearby inner retinal neurons. 30 μm-thick implants with pixel sizes of 280, 140 and 70 μm were successfully implanted in the subretinal space of wild type (WT, Long-Evans) and degenerate (Royal College of Surgeons, RCS) rats. Optical Coherence Tomography and fluorescein angiography demonstrated normal retinal thickness and healthy vasculature above the implants upon 6 months follow-up. Stimulation with NIR pulses over the implant elicited robust visual evoked potentials (VEP) at safe irradiance levels. Thresholds increased with decreasing pulse duration and pixel size: with 10 ms pulses it went from 0.5 mW/mm^2 on 280 μm pixels to 1.1 mW/mm^2 on 140 μm pixels, to 2.1 mW/mm^2 on 70 μm pixels. Latency of the implant-evoked VEP was at least 30 ms shorter than in response evoked by the visible light, due to lack of phototransduction. Like with the visible light stimulation in normal sighted animals, amplitude of the implant-induced VEP increased logarithmically with peak irradiance and pulse duration. It decreased with increasing frequency similar to the visible light response in the range of 2 - 10 Hz, but decreased slower than the visible light response at 20 - 40 Hz. Modular design of the photovoltaic arrays allows scalability to a large number of pixels, and combined with the ease of implantation, offers a promising approach to restoration of sight in patients blinded by retinal degenerative diseases.

Keywords: retinal prosthesis, retinitis pigmentosa, photodiode, retinal degeneration

1. Introduction

Retinitis Pigmentosa (RP) is the leading cause of inherited blindness in the young population, and currently there is no effective treatment. Age-related macular degeneration (AMD) is the major cause of vision loss in people over 65 in the Western world[1]. Development of wet-type AMD and associated vision loss can be slowed down using monthly injections of anti-VEGF agents[2,3], but there remains no cure, as there is no treatment for the dry form of AMD. As the life expectancy increases, the age-related vision loss is becoming a critical issue. National Eye Institute estimates nearly 3M people in the US will have moderate to severe vision loss due to retinal degenerative diseases by 2020[1]. In these blinding conditions photoreceptors degenerate, yet the inner retinal neurons (inner nuclear and ganglion cell layers) that process the visual signals and relay them to the brain are relatively well preserved[4-6].

There are several strategies to transfer visual information to the blinded retina, the two major ones are electrical stimulation of retinal neurons with electrode arrays positioned either epiretinally or subretinally. Excitation of retinal ganglion cells (RGCs) by electrodes positioned on the epiretinal surface bypasses inner retinal circuitry

and requires high frequency stimulation to elicit burst responses[7,8]. Since epiretinal electrodes are positioned on top on the nerve fiber layer and axonal stimulation thresholds are similar to that of RGC somas[9], axonal stimulation is hard to avoid. It is likely the cause of arcuate or wedged visual percepts in patients stimulated with single epiretinal electrodes[10]. In addition, the RF-powered epiretinal system is very bulky: it includes the extraocular receiving coil and signal decoding electronics box connected to the stimulation array via trans-scleral cable. Implantation of such a system is rather complex, with 30% of patients reporting implant-related complications[11]. The best visual acuity obtained with this system so far was about 20/1260[12]. Scaling such an approach to a much larger number of pixels is very challenging.

Although surgically more invasive, placement of electrodes into the subretinal space to stimulate bipolar cells has the potential advantage that the electrical pulse is processed by retinal circuits, converting it into the more natural bursting patterns of the RGCs. This approach is adopted by several groups, including the Retina Implant AG, where a subretinal video camera having 1500 pixels (70 μm in size) is used to convert images into local electric current in each pixel, to stimulate the retina[13]. Power is provided via a cable that exits the eye, and is routed under the skin to behind the ear. A trans-dermal magnetic coupler delivers the power to the receiver, as in a cochlear implant[14,15]. In addition to high pixel density, a major advantage of this system is in the photosensitive nature of the implant, obviating the need for an external video camera to capture the images. Disadvantages of the device include a complex surgery involving many structures of the eye, the orbit and the skull, and a limited dynamic range of ambient illumination enabling normal operation of the intraocular camera. Despite its high pixel density the best reported visual acuity with this system was not much better than with the 60 electrode epiretinal array: 20/1200, although a recent unpublished report indicated a new patient with acuity of 20/550[29].

Peripheral vision is often preserved in AMD patients, which helps maintain their visual acuity at the level of about 20/400, with off-center fixation. This major group of low-vision patients would benefit from a retinal prosthesis if it would provide visual acuity of about 20/200 or better.

To overcome the complexity of the RF-powered systems and to fully utilize the remaining retinal signal processing capabilities, our approach is photovoltaic and subretinal[16]. Images of the visual scene acquired by video camera are processed and projected by video goggles onto a subretinally placed photodiode array using pulsed near-IR (~ 900nm) light. Photovoltaic pixels in the array convert pulsed light into biphasic pulses of electric current that stimulate retinal neurons (primarily in the inner nuclear layer, INL). This system offers several advantageous features: thousands of pixels in the implant can be activated simultaneously and independently; since the pixels are activated by light, no wires are involved, which greatly simplifies the surgical procedure; an external camera allows operation over a wide range of ambient illumination and provides user-adjustable image processing; the optical nature of the device maintains the natural link between eye movements and image perception; and a modular implant design allows implantation via a small retinotomy, while tiling multiple modules permits expansion of the stimulated field. Several prototypes of the photodiode array were developed based on prior experimental and theoretical work[17-19] with pixel sizes of 280, 140 and 70 μm and corresponding electrode diameters of 80, 40 and 20 μm (**Fig 1a**). Each pixel is composed of 3 photodiodes in series, connected between the active and return electrodes[16,20]. In-vitro studies of retinal stimulation with these arrays demonstrated stimulation thresholds ranging from 0.3 to 0.9 mW/mm^2 with pulses from 4 to 1 ms in duration, respectively)[16]. Encouraged by these results we assessed the *in vivo* retinal response to chronically implanted photodiode arrays in rats with normal and degenerate retinas.

2. Methods

2.1 Implant fabrication

Fabrication process of the implant is described in detail elsewhere[20]. Briefly, the array was fabricated on lightly boron-doped silicon-on-insulator (SOI) wafers. The 30 μm thick device can absorb a significant fraction (~70 %) of the NIR light, while still being thin enough to be implanted underneath the retina. Each pixel has 3 photodiodes

connected in series between the central active and circumferential return electrodes. Pixels are separated by 5 μm-wide trenches to improve electrical isolation and to allow nutrient flow through the implant. Photodiodes convert light into electric current with efficiency of about 0.36 A/W/diode[20]. Electrodes are coated with iridium oxide to maximize the charge injection capacity. Scanning electron microscopic of a photodiode array implanted over porcine retinal pigment epithelium is shown in **Fig. 1a**.

2.2 Surgical Procedures

All animal care and experiments were carried out in accordance with the ARVO guidelines for the Use of Animals in Ophthalmic and Vision Research and approved by the Stanford Administrative Panel on Laboratory Animal Care.

Animals were operated on at a mean age of 79 days (range 50-120 days), and recording starting two weeks after the implantation. Subretinal implantation technique was similar to the previously reported one by our group[21]. Briefly, a 1.5 mm incision was made through the sclera and choroid 1.5 mm posterior to the limbus, and the implant was placed into the subretinal space using a custom-made implantation tool. The sclera and conjunctiva were sutured with nylon 10-0 and topical AB (polymixin B) was applied on the eye post operatively. Results obtained with 27 animals are reported in this paper.

2.3 In Vivo Imaging

Anatomical integration of the device into the subretinal space was evaluated by OCT (HRA2-Spectralis, Heidelberg Engineering, Heidelberg, Germany) in consecutive examinations beginning 1 week post surgery. HRA2-Spectralis system (cSLO at 488-nm blue excitation and 500 nm green emission filters) was used for both autofluorescence imaging and for fluorescein angiography, following intraperitoneal injection of 0.2mg/Kg Fluorescein Sodium diluted in Balanced Salt Solution.

2.4 Implantation of the VEP Electrodes

Three skull screw electrodes were implanted similarly to the previously published technique[22] and secured in place with cyanoacrylate glue and dental acrylic. Two electrodes were placed over the visual cortex of both hemispheres, 4mm lateral from midline, 6 mm caudal to the bregma. One reference electrode was implanted 2 mm right to the midline and 2 mm anterior to the bregma. Nose and tail needle electrodes

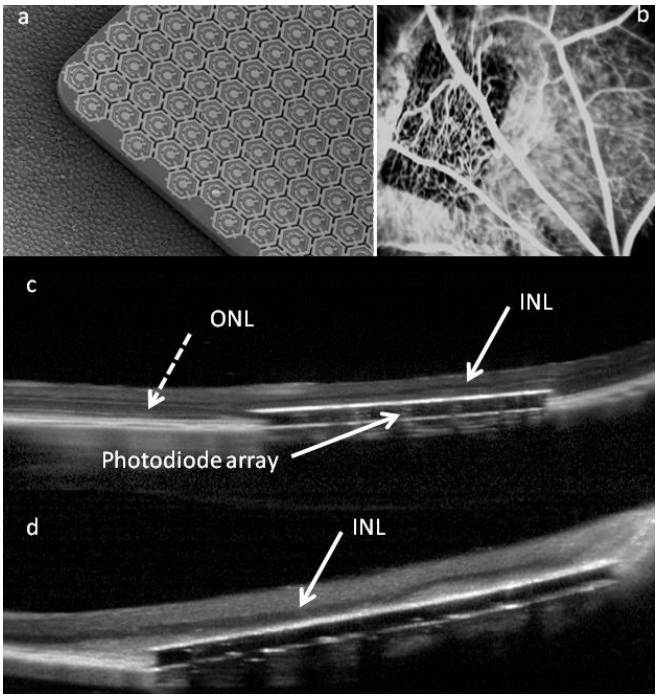

Figure 1. a. Scanning Electron Micrograph of a photodiode array with 70 μm pixels above the RPE in a porcine eye. **b**. Fluorescein angiography 10 days after subretinal implantation of the photodiode array shows good perfusion over the implant with no staining or leakage. **c**. Optical coherence tomography (OCT) of a WT rat 12 weeks after subretinal implantation. INL (pointed by the arrow) is in close proximity to the implant, with no evidence of retinal edema or injury. Photoreceptor layer above the implant is missing due to prolonged separation from the RPE. Implant appears 77 μm thick instead of actual 30 μm due to much higher refractive index of silicon (n≈3.6) than that of ocular tissues (n≈1.4). **d**. OCT of an RCS rat 7 days after implantation. INL (indicated by the arrow) is in close proximity to the implant. As expected, due to retinal degeneration, there is no photoreceptor layer.

served as a reference and the ground, respectively.

2.5 Stimulation and recording

Rats were anaesthetized with a mixture of Ketamine (0.375 mg/kg) and Xylazine (0.125 mg/kg) injected intraperitoneally. The following steps were taken to assure steady anesthesia: spontaneous eye movements and respiratory pattern were checked periodically; additional injections of the 50% of the initial dose were administered every 40 minutes, or as needed, The laser projection system included NIR (915nm) and visible light (635nm) laser diodes coupled into a 1mm optical fiber mounted on a slit lamp (LaserLink, Lumenis Inc.). Following the pupil dilation and eye retraction for optimal alignment of the implant, a small glass cover slip with viscoelastic material was applied to optically flatten the rat cornea and enable imaging of the subretinal implant and focusing of the laser beam. Position of the beam during the experiments was monitored by CCD camera mounted on the same slit lamp. The 635 nm laser was used for aiming and as a visible light source for VEP recordings. Full field white stimuli were provided by the Ganzfeld dome (Espion E2, Diagnosys, Westford, MA, USA) using flashes at 2Hz. 250-500 trials were averaged for each set of parameters. Dome irradiance was varied in the range of 0.01-12.5 cd/m^2. VEP signals were recorded by Espion E2 system (Diagnosys, Westford, MA). Data was acquired at 1 kHz with no temporal filtering. A threshold VEP response was set at 3 standard deviations above the noise level during the first 100 ms after the stimulus. The noise level was defined as the RMS value calculated from the data recorded during the 50 ms preceding the stimuli. Amplitude of the response was measured from the minimum value at N1 peak to the maximum at P2 peak (N1-P2). The frequency response of the VEP was studied with NIR pulses of 10ms in duration and 10mW/mm^2 peak irradiance, and with visible pulses of 10ms in duration and 3.4mW/mm^2 irradiance, applied at 2, 5, 10, 20 and 40 Hz. VEP amplitude for each animal in these measurements was normalized by the amplitude at 2 Hz.

3. Results

3.1 Anatomy of Subretinal Implantation

Eight arrays with pixel sizes of 280μm, 9 with 140μm and 10 with 70μm pixels were successfully implanted subretinally in 27 rats (see Methods): 12 wild-type (Long-Evans) and 15 animals with retinal degeneration (RCS). Follow-up with OCT imaging revealed gradual resolution of mild retinal edema or retinal detachment within the first few weeks after implantation. Figure 1c shows a typical OCT image of an implant in the subretinal space. Due to the much higher refractive index of silicon (n≈3.6) than that of ocular tissues (n≈1.4), the implant appears 2.5 times thicker than it actually is: 77 μm instead of 30 μm. The upper surface of the implant is in close proximity to the INL, where the target neurons for electrical stimulation (bipolar cells) reside. Fluorescein angiography revealed normal vasculature and good perfusion of the retina overlying the implants (**Fig 1b**). Since the Si array blocks visible light, there is no fluorescent background from the choroid, which improves visibility of the retinal vasculature above the implant. As expected, the presence of the implant between the RPE and photoreceptors in wild type (WT) animals caused gradual degradation and disappearance of the photoreceptors above the implant (**Fig 1c**). In 7 out of 12 cases of WT rats we found fluorescent deposits above the implant, beginning a few weeks following the implantation. These are likely associated with degeneration of photoreceptors detached from the RPE by the implant. In RCS rats OCT shows the absence of the photoreceptor layer (Fig 1**d**), and diffuse autofluorescence was distributed over the whole retina, as part of the degenerative process[23]. There were no cases of infection or inflammatory reaction during the 6 months of follow up.

3.2 Visual Evoked Potentials

Typical eVEP response to photovoltaic stimulation was characterized by two early negative components at 15-21ms (N1) and 35-41ms (N2), followed by two positive peaks at 30-35ms (P1) and 55-60ms (P2). A later smaller positive peak (P3) typically had latency exceeding 100ms (**Figure 2a**). VEP response to the natural photopic stimuli was obtained with a 1 mm spot (same size as the implant) of red (635 nm) light projected away from the implant had generally similar structure (N1, P1, N2, P2, P3), but was delayed compared to the response to photovoltaic stimulation (**Figure 2b**). Thought the latency of N1 decreased with increased irradiance (**Figure 3d**), the shortest latency observed was 40 ms – about 20 ms later than the first negative peak in photovoltaic stimulation. This difference is likely due to that fact that electrical stimulation elicits responses from the inner retinal neurons, bypassing the phototransduction process in the retina, which can takes several tens of milliseconds[24]. It should be noted that much brighter light at 635 nm was required to elicit VEP responses equivalent in amplitude to those from the full-field white light illumination (dome). This difference is likely due to at least two factors: much lower sensitivity of rodent retina at 635 nm as compared to white light[25], and smaller area of the illuminated retina. It is quite possible that red light scattered from the small illuminated spot activated the whole retina in the eye.

The eVEP recorded from RCS rats had similar structure to that of the WT rats (Figure 2c). However, the VEP in response to white light in RCS rats was very weak and slow, with no significant N1, even with very bright full-field stimuli. Visible light stimulation with 1mm spot did not elicited any detectable VEP (data not shown).

Stimulation thresholds were determined as the minimum peak irradiance eliciting VEP signal with amplitude 3 standard deviations above the noise level (see detailed description in *Methods*). The lowest threshold in this series was 0.25mW/mm^2 at 4ms, observed in a WT animal implanted with 140 μm pixel array. On average, the thresholds increased with decreasing pixel size: from 0.43 mW/mm^2 with the 280 μm pixels to 1 mW/mm^2 with the 140 μm arrays, and to 2.1 mW/mm^2 with the implants having 70 μm pixels. Thresholds decreased, on average, by a factor of 1.8 when pulse duration increased from 4 to 10 ms. There was no statistically significant difference between the stimulation thresholds in RCS and in WT rats.

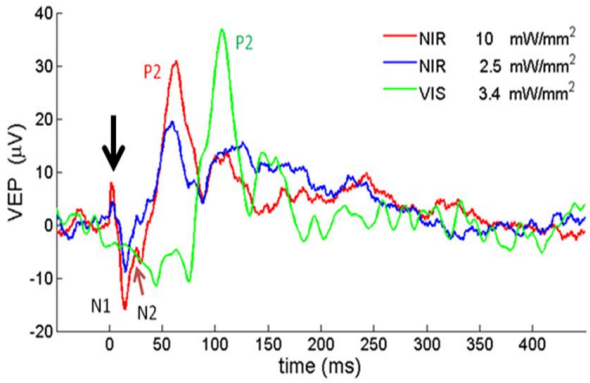

Figure 2. IR stimuli over the implant with 280μm pixels elicited a prompt eVEP with N1 and P2 at 15 ms and 53 ms, respectively. Amplitude of both N1 and P2 increased at higher irradiances. VEP (green) elicited by visible (635nm) light projected onto 1 mm spot away from the implant and eVEP (blue and red) were recorded in the same WT animal. eVEP were recorded in response to 4 ms NIR stimuli at peak irradiances of 2.5 (blue) and 10 mW/mm^2 (red), repeated at 2 Hz. eVEP N1 and N2 had significantly shorter latency as compared to the corresponding VEP latencies. A short artifact caused by the photovoltaic current is indicated by an arrow.

Simultaneous pulsed stimulation of the retina with patterns representing visual scenes is more similar to stroboscopic vision rather than to the natural continuous illumination. At sufficiently high frequencies the pulsed stroboscopic representation fuses into a continuous perception[26]. We assessed potential differences in frequency response to pulsed electrical and visible light stimuli by measuring the amplitude of VEP (N1 to P2) at various pulse repetition rates (**Fig 4**). VEP amplitude, in response to electrical stimulation, decreased with increasing frequency from 2 to 20 Hz similarly to the visible light-induced response (**Fig 4**). From 20 to 40 Hz the visible response continued to decrease, while the eVEP did not change as much. The electrophysiological response of the WT and RCS rats remained stable during the 6 month-long follow up, with variation of the VEP waveforms affected primarily by the state of anesthesia and, in some cases, corneal edema.

4. Discussion

Robust eVEP responses to photovoltaic subretinal stimulation suggest that visual information elicited by the implant in the retina arrives at the visual cortex. Cortical responses could be modulated by both light intensity and pulse width, similar to modulation of the retinal ganglion cells (RGC) responses *in vitro*[18]. Like with visible light stimulation, the RGC spiking rate was gradually increasing with stronger electrical stimuli, indicating preservation of the retinal network signal processing, at least to some extent[18]. Gradual increase in eVEP with stronger stimuli for both, visible light and subretinal electric pulses, shown in the current study, further illustrate similarity of the visual system responses to pulsed visible light and subretinal electrical stimulation. Both, pulse duration and brightness control can be used for modulation of the image in NIR projection systems. Liquid crystal displays (LCD) allow modulation of light intensity with constant pulse duration in each pixel, while Digital Light Processing (DLP) micro-mirror arrays allow pulse duration control with constant light intensity in each pixel. The latter approach should enable rapid sequential activation of pixels, potentially reducing cross talk between adjacent electrodes[27]. In addition, the image can be controlled with Spatial Light Modulators, providing higher throughput and allowing amplitude or duration modulation in each pixel[28].

Stimulation thresholds increased with decreasing pixel size, which may have several potential causes: shallower penetration of electric field with smaller electrodes (as return electrode is closer), lower fraction of open silicon for light collection or reduced number of neurons affected by stimulation with smaller electrodes. With smallest pixels (70 μm), the average stimulation threshold with 4ms pulses were 3.78 mW/mm^2, 53 times below the ocular safety limit for single pulse exposure (200 mW/mm^2 at 900 nm)[16,18]. With repetition rate of 7.5 Hz, the perceptual limit of subretinal stimulation in human patients[29], the average retinal irradiance is about 0.11 mW/mm^2, 47 times lower than the ocular safety limit for prolonged exposures (5.2 mW/mm^2)[18]. Current implants generate cathodic-first electric pulses. Anodic pulses have lower stimulation thresholds in subretinal approach: by a factor of 2-7 [30]. Lower stimulation thresholds are therefore expected with anodic version of the photovoltaic array.

Latency (N1) of the visible light-evoked responses decreases with increasing irradiance due to reduced integration time in photoreceptors[24,31]. In our setup it reached 35 ms at highest measured brightness level (Figure 3). Phototransduction is bypassed during electrical stimulation of the inner retinal neurons, resulting in an earlier appearance of N1, by at least 15 ms, compared to the visible light stimulation. Direct stimulation of RGCs in the epiretinal approach, bypassing the inner retinal neurons, also resulted in an shorter VEP latencies, compared to visible light responses[32].

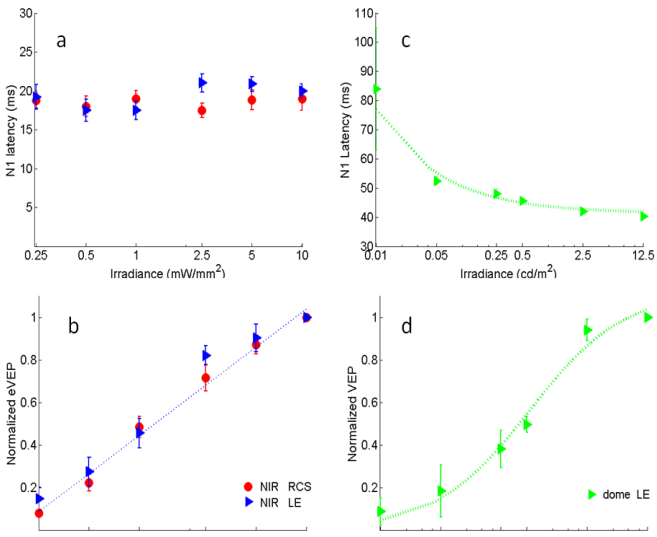

Figure 3. VEP amplitude and latency as a function of peak irradiance for NIR and Visible stimuli. **a**. Averaged N1 latency for 7 WT and 7 RCS rats is plotted as a function of peak irradiance. Pulse duration was held constant at 10ms . did not vary with irradiance, and was very similar in the two animal groups. **b**. The eVEP amplitude (N1-P2), normalized to response at 10mW/mm2 in the same eVEP recordings. The eVEP amplitude increased logarithmically with peak irradiance, with no significant difference between the two animal types. **c**. N1 latency as a function of the peak irradiance in WT rats, in response to white light full-field stimuli, averaged over six animals, and plotted as a function of the peak irradiance. **d**. Normalized VEP amplitude in the same data set. For averaging between the animals the VEP amplitude was normalized to the response at maximum irradiance. Error bars represent the standard error of the mean

Similarity in decrease of the VEP amplitude with increasing frequency for visible and photovoltaic stimulation below 20 Hz indicates that it is governed by processes other than phototransduction. A very similar VEP decrease with higher frequencies was also reported for epiretinal[32] and optic nerve stimulation[33] up to 10 Hz. However, at frequencies higher than 20 Hz the eVEP did not decrease as rapidly as visual light response. This difference is likely due to phototransduction delay since its time constant is on the order of 30-40 ms.

It is not immediately clear whether subretinal stimulation induced only the network-mediated response or also direct activation of RGCs. In-vitro, the network-mediated response of RGCs to subretinal stimulation decreased, on average, by a factor of 5 when frequency increased from 1.5 to 40 Hz[34], similar to the VEP drop in the present study. On the other hand, it has been shown that direct stimulation of RGCs can follow frequencies up to 600 Hz[35]. Even though the VEP decrease with frequency in our experiments does not indicate involvement of direct RGC stimulation, the definitive answers will likely require pharmacological experiments in-vivo[36].

Similarity of the implant induced VEP waveforms to the visible light response, including the late components such as P2 and P3, suggests that retinal response to both types of stimuli arrived to the thalamus and visual cortex. Nevertheless, processing of the electrically-induced information in the primary visual cortex and in the higher visual areas might be affected by the highly synchronized response to pulsed electrical stimuli, lack of latency dependence on stimulus intensity, lack of selectivity in the "on" and "off" pathways, and absence of many other aspects of natural retinal signal processing. Future studies will explore the optimal spatiotemporal protocols of retinal stimulation to maximize the spatial and temporal resolution and contrast sensitivity.

Separation of the retina from RPE resulted in degeneration of the photoreceptors above the implant in WT animals, which may serve a convenient localized model of retinal conditions in degenerative diseases. The similar stimulation thresholds in RCS and in WT animals suggest that localized loss of photoreceptors above the implant affects the retinal neural network sensitivity to electrical stimulation similarly to the slow global loss of photoreceptors and RPE in genetic models of retinal degeneration.

In conclusion, we demonstrated that the small implant size and lack of wires makes photovoltaic arrays easy to implant, even in the eyes as small as in rats. The implants were well tolerated in the subretinal space, and stable over the 6 months follow-up. Robust cortical responses could be broadly modulated by irradiance, pulse duration, and frequency, with stimulation thresholds well below the ocular safety limits. eVEP had generally similar shape and amplitude to the visually-evoked responses, although the latency of the first peak was shorter in eVEP due to lack of phototransduction. The eVEP amplitude scaled with NIR irradiance, frequency and pulse duration similarly to the response to pulsed visible light. Similarities in characteristics of the cortical response to electrical subretinal stimulation and pulsed visible light provide encouraging reassurance in feasibility of the photovoltaic approach to retinal prosthetics. The modularity and scalability of the photovoltaic arrays to a large number of pixels offers a promising approach to functional restoration of sight in patients suffering from blinding degenerative retinal diseases.

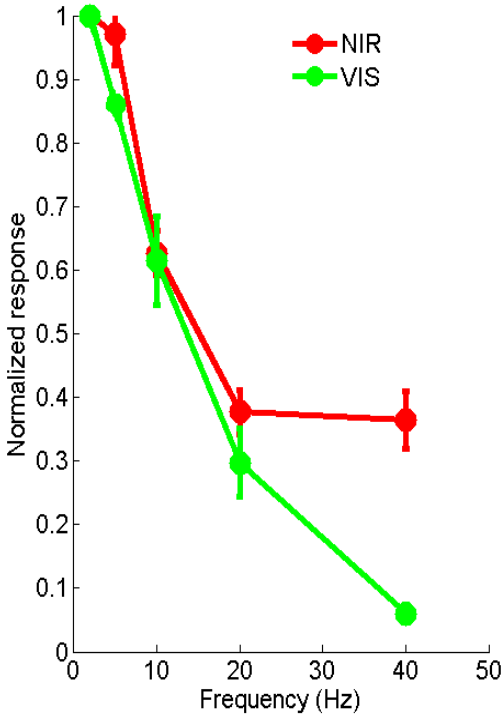

Figure 4. VEP at various frequencies of 1mm visible (635nm) spot projected onto the retina and NIR stimuli. Normalized amplitude of VEP in response to NIR (red, averaged for n=18) and visible (green, averaged for n=6) stimuli at frequencies of 2-40 Hz. Error bars represent standard error of mean.

REFFERENCES

[1] Friedman, D.S., et al., "Prevalence of age-related macular degeneration in the United States," Arch Ophthalmol," 122(4),564-72 (2004)

[2] Martin, D.F., et al., "Ranibizumab and bevacizumab for neovascular age-related macular degeneration," N Engl J Med, 364(20),1897-908 (2011)

[3] Martin, D.F., et al., "Ranibizumab and Bevacizumab for Treatment of Neovascular Age-Related Macular Degeneration: Two-Year Results," Ophthalmology 119(7),1388-98 (2012).

[4] Mazzoni, F., E. Novelli, and E. Strettoi, "Retinal ganglion cells survive and maintain normal dendritic morphology in a mouse model of inherited photoreceptor degeneration," J Neurosci. 28(52),14282-92 (2008).

[5] Kim, S.Y., et al., "Morphometric analysis of the macula in eyes with disciform age-related macular degeneration," Retina 22(4),471-7 (2002).

[6]. Stone, J.L., et al., "Morphometric analysis of macular photoreceptors and ganglion cells in retinas with retinitis pigmentosa," Arch Ophthalmol 110(11),1634-9 (1992).

[7] Nanduri, D., et al., "Frequency and amplitude modulation have different effects on the percepts elicited by retinal stimulation," Invest Ophthalmol Vis Sci. 53(1),205-14 (2012)

[8] Humayun, M.S., et al., "Pattern electrical stimulation of the human retina. Vision Research," 39(15),2569-2576 (1999).

[9] Rizzo, J.F., 3rd, et al., "Perceptual efficacy of electrical stimulation of human retina with a microelectrode array during short-term surgical trials," Invest Ophthalmol Vis Sci 44(12),5362-9 (2003).

[10] Nanduri, D., et al. "Percept Properties of Single Electrode Stimulation in Retinal Prosthesis Subjects. in ARVO abstract. Ft Lauderdale (2009).

[11]. Humayun, M.S., et al., Interim results from the international trial of Second Sight's visual prosthesis," Ophthalmology 119(4),779-88 (2012).

[12] Humayun MS, D.J., da Cruz L, Dagnelie G, Sahel JA, , "Interim results from the international trial of Second Sight's visual prosthesis," Ophthalmology 119(4),779-88 (2012).

[13] Zrenner, E., et al., "Subretinal electronic chips allow blind patients to read letters and combine them to words," Proc Biol Sci 278(1711),1489-97 (2011).

[14] Kakkar, V., "Low Power Architecture For Cochlear Implant," International Journal of Engineering Science and Techn 2(2),51-58 (2010).

[15] Wang, Z., S. Mai, and C. Zhang. "Power Issues on Circuit Design for Cochlear Implants,[4th IEEE International Symposium on Electronic Design, Test and Applications], IEEE Computer Society (2008).

[16] Mathieson, K., et al., "Photovoltaic Retinal Prosthesis with High Pixel Density," Nature Photonics 6(6),391–397 (2012).

[17] Loudin, J.D., et al., "Optoelectronic retinal prosthesis: system design and performance," J Neural Eng, 2007. 4(1): p. S72-84.

[18] Loudin, J.D., et al., "Photodiode Circuits for Retinal Prostheses," Biomedical Circuits and Systems, IEEE Transactions on 5(5),468-480 (2011).

[19] Palanker, D., et al., "Design of a High Resolution Optoelectronic Retinal Prosthesis" Journal of Neural Engineering 2,S105–S120 (2005).

[20] Wang, L., et al., "Photovoltaic retinal prosthesis: implant fabrication and performance," Journal Neural Engineering 9,046014 (11pp) (2012).

[21] Butterwick, A., et al., "Effect of shape and coating of a subretinal prosthesis on its integration with the retina," Exp Eye Res 88(1),22-9 (2009).

[22] You, Y., et al., "Latency delay of visual evoked potential is a real measurement of demyelination in a rat model of optic neuritis," Invest Ophthalmol Vis Sci. 52(9),6911-8 (2011).
[23] Katz, M.L., G.E. Eldred, and W.G. Robison, Jr., "Lipofuscin autofluorescence: evidence for vitamin A involvement in the retina," Mech Ageing Dev,39(1): p. 81-90 (1987).
[24] Lamb, T.D. and E.N. Pugh, Jr., "Phototransduction, dark adaptation, and rhodopsin regeneration: the proctor lecture,". Invest Ophthalmol Vis Sci. 47(12),5137-52 (2006).
[25] Jacobs, G.H., J.A. Fenwick, and G.A. Williams, "Cone-based vision of rats for ultraviolet and visible lights,". J Exp Biol, 204,2439-46 (2001).
[26] Wells, E.F., et al., "Critical flicker frequency responses in visual cortex," Exp Brain Res. 139(1),106-10 (2001).
[27] Wilke, R., et al., "Spatial resolution and perception of patterns mediated by a subretinal 16-electrode array in patients blinded by hereditary retinal dystrophies," Invest Ophthalmol Vis Sci. 52(8),5995-6003 (2011).
[28] Golan, L., et al., "Design and characteristics of holographic neural photo-stimulation systems," J Neural Eng. 6(6),066004 (2009).
[29] Zrenner, E., "Safety and efficacy of the retinal micro-chip in RP and AMD", ARVO Abstract Ft Lauderdale, (2012).
[30] Jensen, R.J. and J.F. Rizzo, 3rd, "Thresholds for activation of rabbit retinal ganglion cells with a subretinal electrode," Exp Eye Res. 83(2),367-73 (2006).
[31] Maunsell, J.H., et al., "Visual response latencies of magnocellular and parvocellular LGN neurons in macaque monkeys," Vis Neurosci. 16(1),1-14 (1999).
[32] Nadig, M.N., "Development of a silicon retinal implant: cortical evoked potentials following focal stimulation of the rabbit retina with light and electricity," Clin Neurophysiol. 110(9),1545-53 (1999).
[33] Li, L., et al., "Intraorbital optic nerve stimulation with penetrating electrodes: in vivo electrophysiology study in rabbits," Graefes Arch Clin Exp Ophthalmol. 247(3),349-61 (2009).
[34] Jensen, R.J. and J.F. Rizzo, 3rd, "Responses of ganglion cells to repetitive electrical stimulation of the retina," J Neural Eng. 4(1), S1-6 (2007).
[35] Cai, C., et al., "Response variability to high rates of electric stimulation in retinal ganglion cells," J Neurophysiol. 106(1),153-62 (2011).
[36] Shah, H.A., et al., "Electrical Stimulation of the Rabbit Retina With a Sub-Retinal Electrode Array: Charge and Charge Density Limits for Safe Stimulation," ARVO. Invest Ophthalmol Vis Sci,46: E-Abstract 1507 (2005).